CANADA

DEPARTMENT OF
ENERGY, MINES AND RESOURCES
MINES BRANCH
OTTAWA

THE MECHANICAL PROPERTIES OF ZINC SINGLE CRYSTALS AT HIGH STRAIN RATES

A. SCHWEIGHOFER AND F. W. MARSH

PHYSICAL METALLURGY DIVISION

NOVEMBER 1966

1867 1967

Research Report R 186

Price 75 cents

Available by mail from the Queen's Printer, Ottawa,
and at the following Canadian Government bookshops:

OTTAWA
Daly Building, Corner Mackenzie and Rideau

TORONTO
Mackenzie Building, 36 Adelaide St. East

MONTREAL
Aeterna-Vie Building, 1182 St. Catherine St. West

or through your bookseller

A deposit copy of this publication is also available
for reference in public libraries across Canada

Price 75 cents Cat. No. M38-1/186

Price subject to change without notice

ROGER DUHAMEL, F.R.S.C.
Queen's Printer and Controller of Stationery
Ottawa, Canada
1967

Mines Branch Research Report R 186

THE MECHANICAL PROPERTIES OF ZINC SINGLE CRYSTALS AT HIGH STRAIN RATES

by

A. Schweighofer* and F. W. Marsh**

- - - - - - - -

ABSTRACT

Mechanical properties of zinc single crystals when subjected to a strain rate of 10^4 sec^{-1} at room temperature were studied. Specimens were loaded in a drop-weight machine, and simultaneous load and deformation measurements were made electronically. Three groups of specimens were tested, the first with basal plane orientations close to the tensile axis, the second close to 45 degrees and the third close to 90 degrees.

Deformation of the first group was due to twinning, the second group exhibited ductile deformation, with pure glide, and the third group failed by cleavage with very short deformation times.

The increased strain rate resulted in decreased total plastic strain, increased coefficient of work hardening and increased fracture stresses.

All properties studied were found to be in good agreement with published results from previous work done at low strain rates and low temperatures.

---

*NRC Post-Doctorate Fellow and **Senior Scientific Officer, Engineering Physics Section, Physical Metallurgy Division, Mines Branch, Department of Energy, Mines and Resources, Ottawa, Canada.

Direction des mines

Rapport de recherches R 186

LES PROPRIÉTÉS MÉCANIQUES DE MONOCRISTAUX DE ZINC À DES VITESSES DE DÉFORMATION ÉLEVÉES

par

A. Schweighofer* et F. W. Marsh**

RÉSUMÉ

Les auteurs ont étudié les propriétés mécaniques de monocristaux de zinc soumis à une vitesse de déformation de 10^4 sec.$^{-1}$ à la température ambiante. Les échantillons ont été placés dans un appareil d'essai par choc et les mesures de charge et de déformation ont été prises simultanément par procédé électronique. Trois groupes d'échantillons ont été soumis aux essais: dans le premier, le plan basal était à peu près parallèle à l'axe de traction; dans le deuxième il était incliné d'environ 45 degrés, et dans le troisième, d'environ 90 degrés, par rapport à cet axe.

La déformation du premier groupe était due au maclage. Le deuxième groupe a subi une déformation ductile accompagnée d'un glissement pur, tandis que le troisième groupe s'est déformé par clivage avec des temps de déformation très courts.

L'augmentation de la vitesse de déformation a entraîné une diminution de la déformation plastique totale, une augmentation du coefficient d'écrouissage, et un accroissement des efforts de rupture.

Les auteurs ont trouvé que toutes les propriétés étudiées concordent avec les résultats publiés de travaux antérieurs effectués à de faibles vitesses de déformation et à de basses températures.

---

*Agrégé post-doctoral au Conseil national de recherches, et **Agent scientifique sénior, Section de la physique appliquée, Division de la métallurgie physique, Direction des mines, ministère de l'Energie, des Mines et des Ressources, Ottawa, Canada.

CONTENTS

INTRODUCTION

From the theoretical and practical point of view, much attention has been devoted to the discrepancy between the theoretical strength of crystals and the observed fracture stresses. For zinc, the theoretical strength is calculated to be about 10^6 g/mm^2, whereas the observed fracture stress is about 6×10^3 g/mm^2, mainly due to the influence of plastic deformation, which precedes every failure, including cleavage fractures.

In spite of the fact that the first research into the mechanism of fracture in metals was in 1935 (Schmid and Boas), systematic studies of zinc fractures were not begun until 1953.

The results obtained by Schmid and Boas[1] on single crystals of zinc, bismuth and tellurium have favoured Sohncke's criterion for the cleavage fracture of single crystals, i.e. that the cleavage occurs only when the component of the stress normal to the cleavage plane reaches a critical value.

However, Deruyttère and Greenough[2] have pointed out that Sohncke's normal stress law is not valid for zinc single crystals with orientations between 12 and 90 degrees. In 1956[3] they suggested that it is unlikely that failure is so affected by prior deformation that a correction for this would give results in accord with Sohncke's law. In zinc single crystals for which the angle between the basal plane and the tensile axis is less than 12 degrees ($X < 12°$), the cleavage process is associated with the development of macroscopic twins, and the cleavage faces are not a single plane but two sets of faces approximately at right angles to each other. It was found that all the cleavage faces in the matrix or in the twins were the (0001) planes (Mathewson and Phillip[4], Deruyttère and Greenough[3]). Bell[5] observed that cracks were often visible in the twins at points remote from the main fracture, and suggested that these cracks in the basal plane of

the twins constituted the initial fracture, and that the cleavage in the matrix follows ("secondary basal cleavage"). The fracture stresses for the secondary basal cleavage compared favourably with those for primary basal cleavage.

The results which were obtained by Gilman[6] for N/X° curves (N = normal stress) are in close agreement with those obtained by Deruyttère and Greenough[2, 3]. He showed that the fracture stress for zinc, in the absence of prior glide, can be as high as about 5500 g/mm^2 at room temperature, and about 4500 g/mm^2 at -196°C.

Bullen[7] is in agreement with the "law of constant normal stress" for the orientation range 18° < X < 55°. For X > 55°, the fracture condition approximates to a constant shear stress law. The normal stress (N), which is responsible for fracturing, is in inverse relationship to the shear strain prior to fracture up to the transition strain.

Investigations have shown that increasing the deformation rate reduces plastic deformation in two ways:

1. as a result of wave interference and inertial forces,
2. in the process of plastic deformation, two fundamentally distinct processes are simultaneously involved in the deformation of a crystal by glide: one concerns the actual crystal and is structurally determined, the other is based on thermal lattice vibrations. During high speed deformation the latter is restrained to a considerable degree.

The effect of strain rate on the elongation before cleavage in pure polycrystalline zinc in tension was studied by Greenwood and Quarrell[8]. The effect of deformation rate within the range from 1 to 1/500%/sec was too small to be detectable below -77°C. Its effect, however, was increasingly marked at higher temperatures, 0°, 10°, and 20°C.

Lucke, Masing and Schroder[9], and Seeger[10] observed an appreciable effect of deformation rate in the range $10^{-6} < \varepsilon < 10^{-1}$ sec^{-1}, on the coefficient of work hardening (θ) in zinc single crystals (99.995% purity). Investigations by Pond and Glass[11], Taborsky[12] and Schweighofer and Kralik[13] on high speed deformation of aluminum single crystals in tension have, in general, confirmed their results.

The present work is a study of the dependence of fracture stresses and strains in zinc single crystals upon orientation at high strain rates, which reduce the amounts of strain occurring before fracture, and increase the non-uniformity of the plastic deformation.

MEASUREMENT TECHNIQUE

A photo-optical method[14] was used for strain determinations. Observations were made of the movement of a small target, in the form of a black isosceles triangle on a white background, fixed to the free end of the specimen (Figure 1). The target was illuminated with a 110 volt 100 watt lamp, excited by a very well regulated and filtered d-c power supply. The image of the target was focussed on a transverse slit, placed immediately in front of a 931-A photomultiplier tube. Thus vertical movement of the target produced a change in voltage output from the photomultiplier. Due to the fast response time and high sensitivity of the photomultiplier, it was essential that target illumination be maintained absolutely constant, and that the optical system be shielded from extraneous light. Vertical position of the slit was controlled by a screw, and slit position was indicated by a dial-gauge. A ten-turn linear potentiometer was mechanically connected to the screw, as shown in Figure 2, to provide a d-c voltage proportional to vertical slit position. Output from the photomultiplier was applied to the vertical deflection plates of one channel of a "Tektronix" model 555 dual beam C.R.O. through a type 1A1 preamplifier, and a single externally triggered sweep was used for each test. With the voltage from the linear potentiometer applied to the horizontal deflection plates, and the

target fix, an s-y plot of slit movement versus photomultiplier output was displayed on the C.R.O. as the screw was rotated. Thus, since the ratio of photomultiplier output with varying slit position (target position fixed) to photomultiplier output with varying target position (slit position fixed) was constant, a simple and convenient method was provided for checking overall calibration of the apparatus. Calibration was effected by adjusting vertical position of the target, in situ, by means of a cathetometer, and recording resultant deflections of the C.R.O. trace. A calibration check was made before each test.

A photo-voltaic cell, illuminated by a small lamp, was fixed to the machine frame in a position such that the drop-weight would interrupt the illumination immediately prior to the application of load on the specimen. The resulting signal was applied to the external trigger input of the C.R.O., and the time interval between triggering and application of load was adjusted by altering the position of the cell, and/or utilizing the delayed sweep of the C.R.O.

Errors induced by misalignment of the target with respect to the optic axis and fluctuations in supply voltages were assessed by making a large number of calibration curves, varying one parameter only, at a time. Parameters considered were: target translation along the optic axis (focus), target rotation about each of the three major axes, anode, and cathode voltages. The largest errors measured occurred with target rotation about the optic axis. Rotations of ±5° from symmetrical target alignment resulted in about ±15% differences in C.R.O. trace deflections, for each vertical position of the target. Rotation of the target about a horizontal axis normal to the optic axis, which was considered to be the most probable misalignment occurring in practice, indicated that errors from this source are very small. Rotations of ±5° resulted in a maximum spread of about 0.25 mm in C.R.O. deflections. Translation of the target along the optic axis (focussing) resulted in errors of +0, -5% for translations of ±0.25 in. In practice, focussing error was found to be less than about ±.02 in. Other errors

were found to be insignificantly small.

Instantaneous specimen loading was measured, simultaneously with deformation, by applying the output of a load-cell to the vertical deflection plates of the other channel of the C.R.O., through a type Q transducer preamplifier. The load-cell consisted of four 1000 ohm foil strain gauges mounted on a hollow steel cylinder in a wheatstone bridge configuration. The load-cell was incorporated in the specimen gripping device in such a manner that a tensile load on the specimen produced an equal load on the load cell. The load-cell was statically calibrated on a compression testing machine, and with dead weights before starting, and at intervals during, the testing program. A calibrating register, built into the type Q unit, permitted checking one point on the calibration curve before each test.

All C.R.O. traces were recorded on photographic film, using a "Polaroid" camera.

APPARATUS

An existing drop-weight machine was modified for use in the tests. The modification consisted of a device, shown in Fiture 3, for holding the specimen, and applying a tensile load to it. The main considerations in designing the device, were incorporation of a load-cell at the fixed end of the specimen, and accurate alignment of a beam at the free end of the specimen to ensure axial loading.

The load-cell consisted essentially of a mild-steel hollow tube of 0.102 $in.^2$ cross section, permitting a maximum load of 3000 lb, which is 7 to 8 times the load required for failure of zinc single crystals of 6 mm diameter.

Concentricity and alignment of the beam was accomplished by locating it between two vertical ground surfaces, with two tapered pins fixed in a horizontal ground surface, the beam was of high strength aluminum alloy, 7075-T6.

The specimens were gripped in the device by pouring Woods metal into two conical cavities, into which the ends of the specimens protruded, as shown in Figure 3.

The gripping device was placed concentrically at the base of the 16 ft high drop-weight testing machine. The drop-weight, reaching a speed of 30 ft/sec on falling from maximum height, delivered 150 ft-lb of energy.

To ensure axial loading of the specimen it was imperative that the drop-weight contact both ends of the beam simultaneously. This was accomplished as far as possible by:

a. reducing the contact area of the weight and beam to a minimum,

b. reducing the distance between the contact areas on the beam to a minimum,

c. restricting the movement of the drop-weight to the axial direction by employing guides, ground to close tolerances, and mounting ball bearings on the weight itself.

Difference in time of contact made by the weight with the two ends of the beam was measured electronically and was found to be 10^{-5} sec corresponding to 0.001% specimen deformation, which is not significant.

SPECIMENS

The material used for the preparation of the zinc single crystals was of 99.999% purity, having the analysis given in Table 1.

TABLE 1

Analysis of Zinc used for Specimens

Pb %	Sn %	Cd %	Fe %	Cu %	As %
0.0001	0.00005	0.00005	0.0004	0.0005	0.000004

The material was in the form of extruded bars. Single crystals, 6 mm in diameter and 150 mm long, with random orientation were grown from the melt in an argon atmosphere, using oblique moulds of precision-bore Pyrex tubing. The moulds were coated internally with graphite (Aquadag) to facilitate removal of the crystals from the tubes. Selected crystals were used as seeds for growing about 50 single crystals, 10 mm in diameter and 180 mm long, with orientations $X = 3° - 9°$, $X = 41° - 59°$ and $X = 84° - 89°$.

The single crystals were cut into 60 mm lengths by means of an acid-saw, using 50% nitric acid in water. A 40 mm gauge length was reduced in section, to a minimum of 6 mm diameter, employing an acid machine[15]. Optimum results were obtained by using 38% nitric acid in water, and 60 rpm. To ensure reliable adhesion of Woods metal at the gripped ends of the specimen, the ends were grooved chemically in the circumferential direction. Uniformity and minimum residual stresses in all specimens were obtained by annealing at 400°F for 2 hours, and allowing specimens to cool in the furnace. The specimens were then chemically polished in Gilman's solution[16].

To check the elongation, two sets of electric-pencil marks, approximately 3 mm apart, were placed along the entire gauge-length and spacings were accurately measured with a travelling microscope.

52 zinc single crystals with the orientations given in Table 2 and illustrated in Figure 5 were tested:

TABLE 2

Testing Schedule

Group	x	Number of Specimens	
		Tested	Acceptable Results
1	3° - 9°	17	8
2	41° - 59°	15	14
3	84° - 89°	20	8

The 22 specimens for which results are not reported all fractured in or near the grips and 90% of such fractures occurred at the free end of the specimen. Such failures are consistent with previous observations[6, 12] and are due to:

1. non-uniform stress distribution due to the high strain rate,
2. inhibition of glide by the grips.

OSCILLOSCOPE RECORDS

For each of the three orientation groups, a markedly different type of load-time curve was recorded.

a. A salient feature of the first group, with low X (3° - 9°), was the typical relaxation in load, at the moment of twin formation (Figure 6). The magnitude of relaxation was found to be dependent upon the volume in which twinning occurred. From the curves obtained for this group, it was possible to measure twinning stress, relaxation stress and fracture stress[17]. Figure 7 indicates the method.

b. Curves for the second group ($41° \leq X \leq 59°$) may be divided into main classes:

(i) Specimens with basal plane orientations close to the [0001] - [11$\bar{2}$0] direction showed ductile deformation with pure glide. The deformation speed was approximately linear with time throughout the entire range at about 8 m/sec (Figure 8).
Note: Although Seeger[18] has suggested that such basal plane orientations produce deformation by pure glide only, present results indicate that in some cases, twinning also occurred (Figure 9).

(ii) Specimens with basal plane orientations in the [0001] - [10$\bar{1}$0] direction with two equal glide directions ($\lambda_1 = \lambda_2$) showed an increase in rate of work hardening, and lowered ductility. However, the time-deformation curve remained essentially linear, and of the same order, 8 m/sec (Figure 10). Some specimens in this class exhibited twinning (Figure 11).

(c) Basal plane orientation of the third group was approximately perpendicular to the tensile axis, and failure was, in some cases, by pure cleavage (Figure 12), and in others, after a very small deformation (Figure 13). Deformation times were very short (0.1 to 0.2 ms).

STRESS-STRAIN CURVES

Dynamic stress-strain curves have been calculated only for crystals with basal plane orientation $41° \leq X \leq 59°$, because only these records are typical for a homogeneous deformation of single crystals.

Curves calculated from a typical oscilloscope record for each of the two classes are shown in Figures 14 and 15. These curves were used to determine the resolved shear stress-shear strain curves shown in Figure 16. It is evident from these curves that, as with results from static tests, the results from high speed deformation tests can be divided into two groups with regard to the coefficient of work-hardening: the first group of crystals

contain one predominant glide direction ($\lambda_1 < \lambda_2, \lambda_3$) for example specimen No. 6-2.

In the second group, critical shear stress is approximately the same in two directions, so that two glide directions can be active simultaneously. The orientations of these is close to the [0001] - [10$\bar{1}$0] direction.

From Figures 17 and 18 it is seen that the shape of the curves is not changed by increasing the deformation rates by up to 10^6 sec^{-1}. Thus, it may be concluded that the mechanism of plastic deformation is not affected qualitatively by strain rates of this order.

Note: The above conclusion should be confirmed by metallographic examination, which has not yet been carried out, but will be reported later.

Although the shapes of the curves are similar, the slopes are seen to differ, indicating that the coefficient of work hardening is higher for higher strain rates. Figures 17 and 18 compare results from the present work with those obtained by Lücke et al[9], who studied the effect of strain rate on work hardening of zinc single crystals with approximately the same orientations, but with a maximum strain rate of 10^{-2} sec^{-1}.

Using maximum strain rates of 10^4 sec^{-1} i.e. approximately 10^6 sec^{-1} higher than used by Lücke et al[9], shear strain in the first group was found to be 60% lower, and in the second group 70% lower than Lücke's values. This may be explained by the increased work hardening produced at the higher strain rates.

Figure 16 shows that the coefficients of work hardening, obtained from the first linear portion of the curves, due to high strain rates are from 650-730 g/mm^2, and for specimen No. B-6 reached a value of 2850 g/mm^2. Table 3 compares results of the present work with those of Lücke et al[9].

TABLE 3

Comparison of Results

	Lücke et al			Present Work
$\dot{a}$ [sec^{-1}]	2×10^{-4}	8×10^{-4}	2×10^{-2}	10^{2}
τ_{crit} [g/mm^2]	57	64	110	220
$\left(\frac{\partial \tau}{\partial \alpha}\right)_{\theta_I}$ [g/mm^2]	53	79	153	600
$\left(\frac{\partial \tau}{\partial \alpha}\right)_{\theta_{II}}$ [g/mm^2]	440	698	900	
$\alpha_{\theta\tau}$ [%]	130	130	140	80

Figure 19 indicates that a single point obtained from the present work agrees favourably with the curve published by Seeger et al[18] when extrapolated to 10^2 sec^{-1}, but that the room temperature coefficient of work hardening does not become asymptotic at the value he suggested.

FRACTURE STRESSES

It would be normally expected that a true cleavage fracture stress could only be measured in the absence of stress concentrations arising during prior plastic flow, that is, in the case of completely brittle behaviour. In practice, there is generally little difference between the cleavage fracture stresses determined from static tests on a completely brittle specimen and those determined from static tests on a specimen that exhibits twinning.

The two groups of crystals with basal plane orientations

$3° \leq X \leq 9°$ and $X \sim 90°$ exhibited essentially cleavage fractures, as seen in the latter case, from the strain magnitudes given in Table 4.

TABLE 4

Fracture Stresses and Elongation for Group 3 Specimens

Crystal	X°	Fracture Stress (g/mm^2)	Elongation (%)
14-3	88	974	1.26
20-1	89	3872	1.71
17-2	87	2727	0.94
17-3	87	2787	1.62
5-3	85	1345	1.48
8-1	84	2141	1.68
8-2	84	2156	2.18

Gilman[16], studying the deformation of cylindrical zinc single crystals at a strain rate of 0.005 per min, obtained the results given in Table 5.

TABLE 5

Fracture Stresses According to Gilman[16]

X°	Fracture Stress (g/mm^2)
88	843
88	1480
88	1150
88	2580
88	2100
89	3140
86	1265
86	2880

Comparing the present work with the results of Gilman and others[3,19], it should be noted that the basal plane was not exactly perpendicular to the stress axis in both cases, resulting in a small component of shear stress on the glide plane, but it may be seen that the fracture stresses tend to increase with strain rates.

In Figure 20, present values of fracture stresses are plotted along with results obtained by Deruyttère and Greenough[3], using crystals of the same diameter. It is apparent that the present results lie on their extrapolated curve of $\sigma_{pf}/X°$, although their work was carried out at -196°C.

Values of normal fracture stress ($\sigma_N = \sigma_o \sin^2 X$) are plotted against basal plane orientation (X), obtained from the present work, and by Deruyttère et al[3] in Figure 21. Since the present values lie along their σ_N/X extrapolated curve, it is seen that σ_N varies by a factor of 70 in the range $15° \leq X \leq 89°$, and that their contention that Sohncke's law is invalid in the range $15° \leq X \leq 83°$ is verified. The fracture stresses of specimens having orientations of basal plane $3° \leq X \leq 9°$ are much lower than those reported by Burr and Thompson[20] at room temperature with low deformation rates, but are in close agreement with the value of 2.7 kg/mm^2, which they obtained by the deformation of zinc single crystals with basal plane orientation $X = 2°$ at 20°K.

TWINNING STRESSES

Twinning in pure zinc occurs by shear on a pyramidal plane Type I order 2, i.e. $(10\bar{1}2)$ and $\langle 10\bar{1}\bar{1} \rangle$ direction. Here we have a single glide plane and six planes of twinning. As has been shown for BCC metals, twinning also occurs in HCP metals most easily on those systems for which the applied stress, when resolved into the twinning plane and along the twinning direction, has the highest value[21]. Examination of the lattice

for specimens of Group 1 shows that the most active planes are in systems T3 and T4 with the directions t4 and t3 (Figure 22). Table 6 gives the values of angles between the tensile axis and twinning planes (X*), and those between tensile axis and twinning direction (λ^*).

TABLE 6

Twinning Angles for 4 Specimens

Crystal	System	X*	λ^*	sin X* cos λ^*
4	T3	36	41	0.442
	T4	52	58	0.416
C-3	T3	36	40	0.449
	T4	53	58	0.442
12	T3			
	T4	50	45	
9	T3	37	41	0.453
	T4	53	57	0.434

Resolved shear stress in a twinning system (σ_{RTWS}) for a given crystal orientation is:

$$\sigma_{RTWS} = \sigma_{TWS}(\sin X^* . \cos \lambda^*)$$

where σ_{TW} = twinning stress.

Results obtained from the tests are given in Table 7. According to Schmid[1] Figure 23, all orientations fall in area "D", so that specimen extension occurs due to twinning on any one of the six twinning planes.

The above mentioned relaxation stress due to twinning (Figure 6), averaged about 40% of the fracture stress, while Cahn and Bell[21] measured a relaxation of only 25%. Metallographic examinations will be made to assess the volume in which twinning occurred.

TABLE 7

Twinning Stresses for Group 1 Specimens

Specimen	Orientation		Twinning Stress (g/mm^2)	Max Resolved Twinning Stress (g/mm^2)
	X	λ		
C-2	9	15	1817	817
C-3	9	15	1717	771
4-2	8	16	1506	666
4-3	8	16	1396	618
9-1	8	16	1480	672
9-2	8	16	1680	762
9-3	8	16	1685	765
12-1	3	25	942	469
12-2	3	25	1296	647
12-3	3	25	1452	726

SUMMARY

During the past decade considerable work has been done in evaluating mechanical properties of zinc single crystals at low strain rates, and in other metals at high strain rates. The present report, based on this information, deals with the experimental investigation of the effect of a strain rate of 10^4 sec^{-1} on some mechanical properties of pure zinc single crystals, in tension. Results of these experiments may be summarized as follows:

1. Increasing the rate of deformation by 10^6 sec^{-1} does not influence the shape of the work-hardening curves. Deformation of specimens with orientations of the (0001) plane close to the tensile axis is due to twinning, and specimens with an orientation close to 45° are ductile.

2. Work-hardening curves, for a high deformation rate, exhibit only one linear portion, similar to those for low deformation rates at low temperatures.

3. Increasing deformation rate, at room temperature, by 10^6 sec^{-1} results in
   (a) Decreased total plastic strain by 60-70%.
   (b) Increased coefficient of work hardening (over the first linear portion) by 300%.
   (c) Increased fracture stresses by approximately 50%.

4. The value obtained for the coefficient of work hardening lies on a smooth extrapolation of the published curve for lower strain rates.

All properties studied in the present work are in good agreement with those previously determined at low deformation rates at 20°K, which suggests that the mechanisms affecting plastic deformation at high strain rates at room temperature, and at low strain rates at low temperatures are similar. This may be confirmed by future metallographical examination of the test specimens.

REFERENCES

1. Schmid E., Boas W.: Kristallplastizität, J. Springer, Berlin (1935).
2. Deruyttère A., Greenough G. B.: Nature 172, p. 170 (1953).
3. Deruyttère A., Greenough G. B.: J. Inst. Metals 84, p. 337 (1956).
4. Mathewson C. H., Phillips A. J.: Trans. AIME Metals Div., p. 143 (1927).
5. Bell R. L., : Ph Tesis, Univ. of Birmingham (1954).
6. Gilman J. J.: Trans Met. Soc. AIME 212, p. 783 (1958).
7. Bullen F. P.: Trans. Met Soc AIME 227, p. 1069 (1963).
8. Greenwood G. W., Quarrell A. G.: J. Inst.Metals 82, p. 551 (1953-54).
9. Lücke K., Masing G., Schröder K.: Z.f. Metallkunde 46, p. 792 (1955).
10. Seeger A.: Z.f. Naturforschung, 11a, p. 985 (1956).
11. Pond R. B., Glass C. M.: Response of Metals to High Velocity Deformation, Inter. Publ. N. Y. p. 145 (1961).
12. Taborsky L.: Kovove materialy 4, p. 3 (1965).
13. Schweighofer A., Kralik F.: Kovove materialy 3, p. 60 (1965).
14. Laroçque, G. E.: Dept. of Mines and Technical Surveys, Mines Branch Div. Rep FMP-65/9 MRL.
15. Washburn J., Parker E. R. : Modern Research Technique in Physic Met. ASM, p. 156 (1953).
16. Gilman, J. J., Carlo V. J.: J. of Metals 8, p. 511 (1956).
17. Harding J.: Nat. Physical Lab., Teddington, Met. Rep. 31, M3296.
18. Seeger A., Träuble H.: Z. f. Metallkunde 51, p. 435 (1960).
19. Jenckel E.: Z. f. Elektrochem. 38, p. 569 (1932).
20. Burr D. J., Thompson N.: Phil. Mag. 12, p. 229 (1965).
21. Bell R. L., Cahn R. W.: J. Inst. of Metals 10, p. 433 (1957-58).

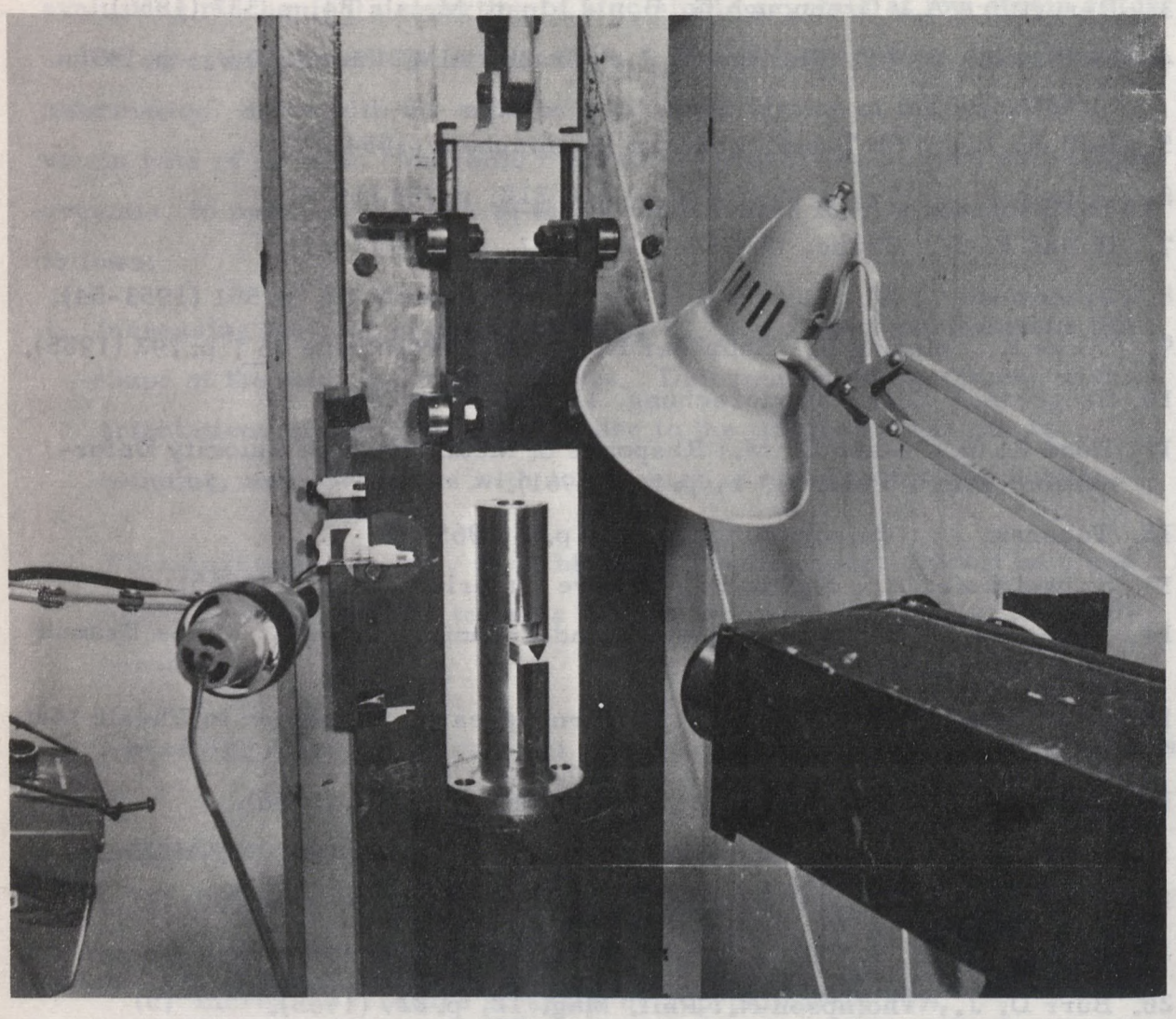

Figure 1. Testing and Measuring Apparatus.

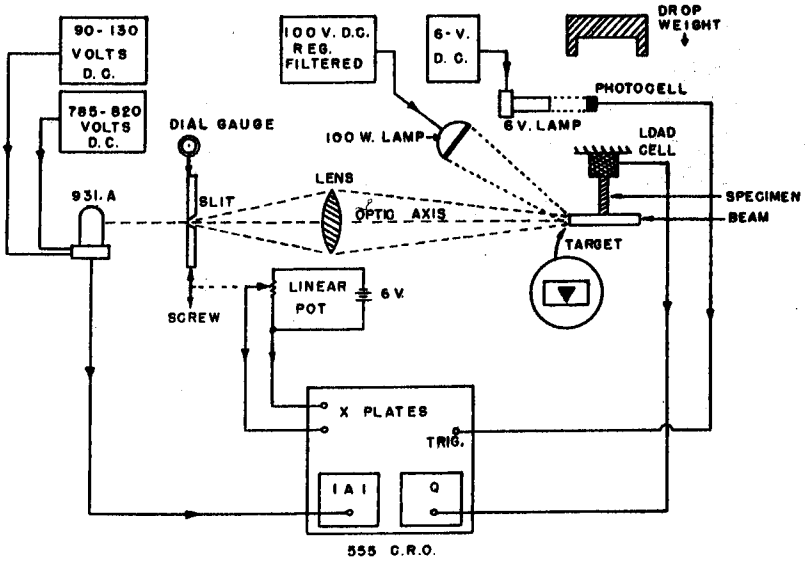

Figure 2. Arrangement of apparatus.

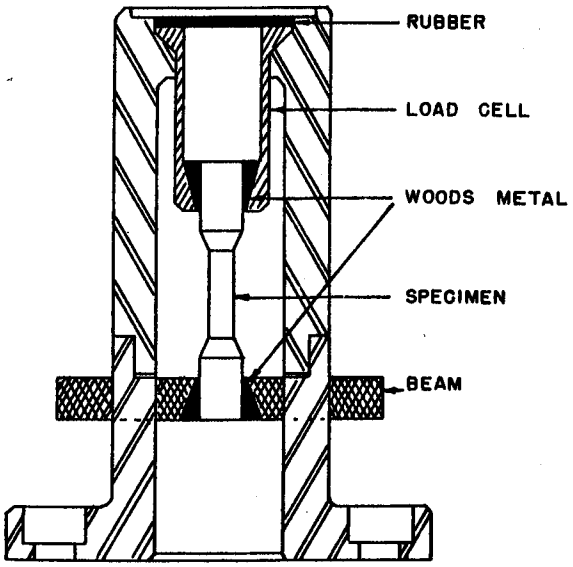

Figure 3. Gripping Device

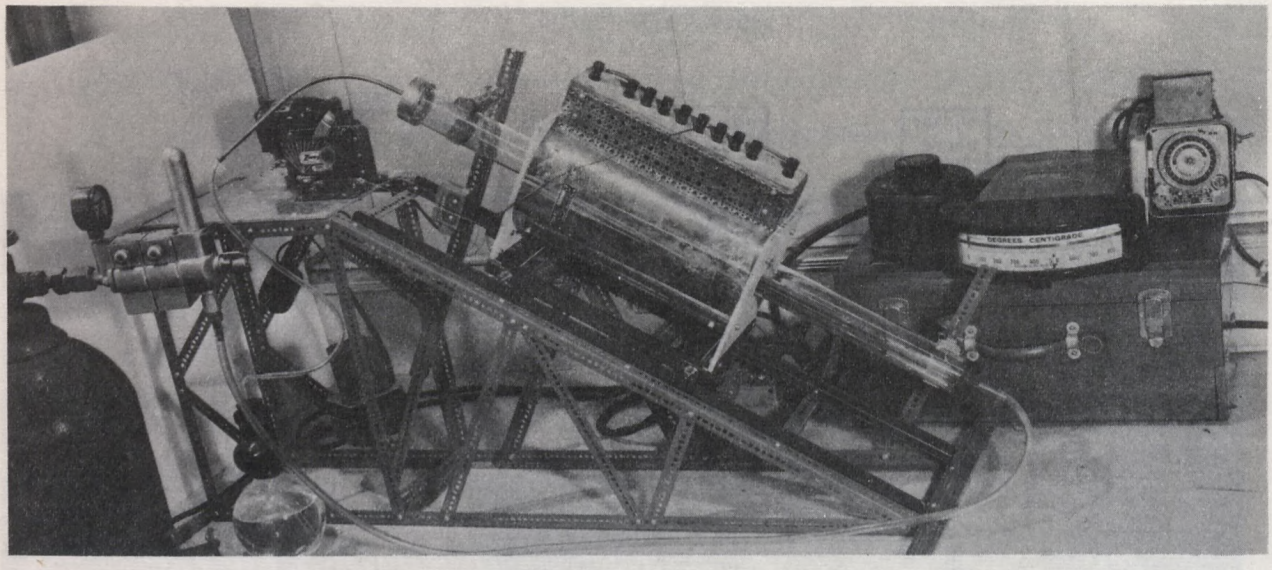

Figure 4. Travelling Furnace.

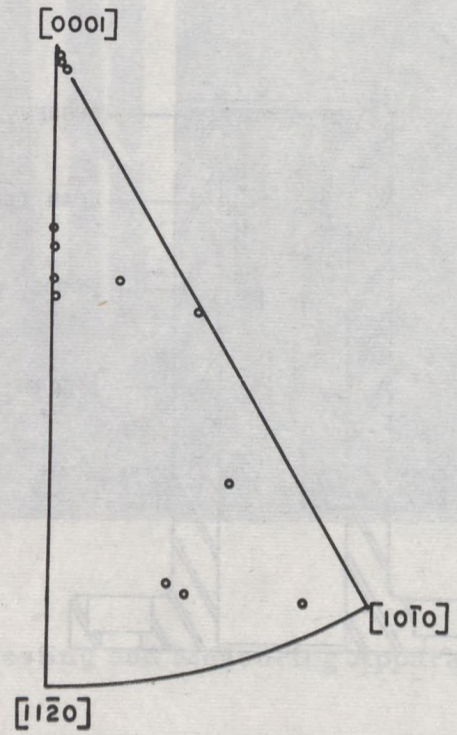

Figure 5. Orientation of Single Crystals Tested.

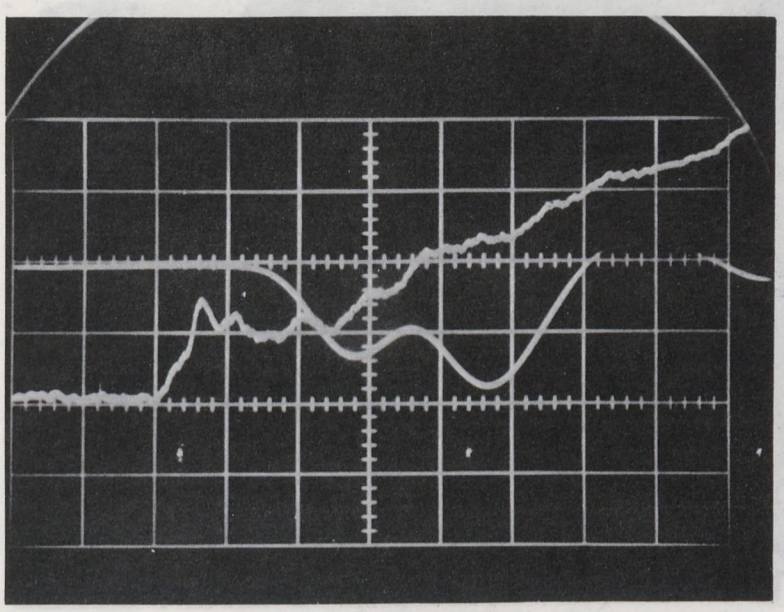

Figure 6. Oscillograph of Brittle Specimen Test showing Twinning.

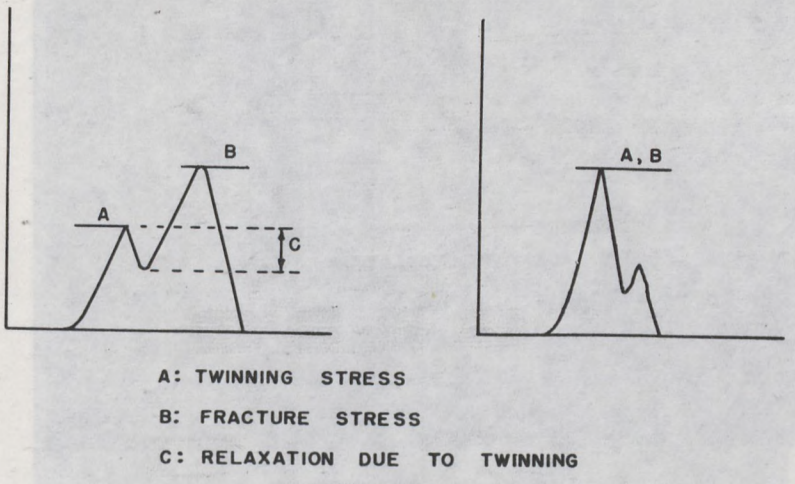

Figure 7. Details of Stress Measurement of Typical Record.

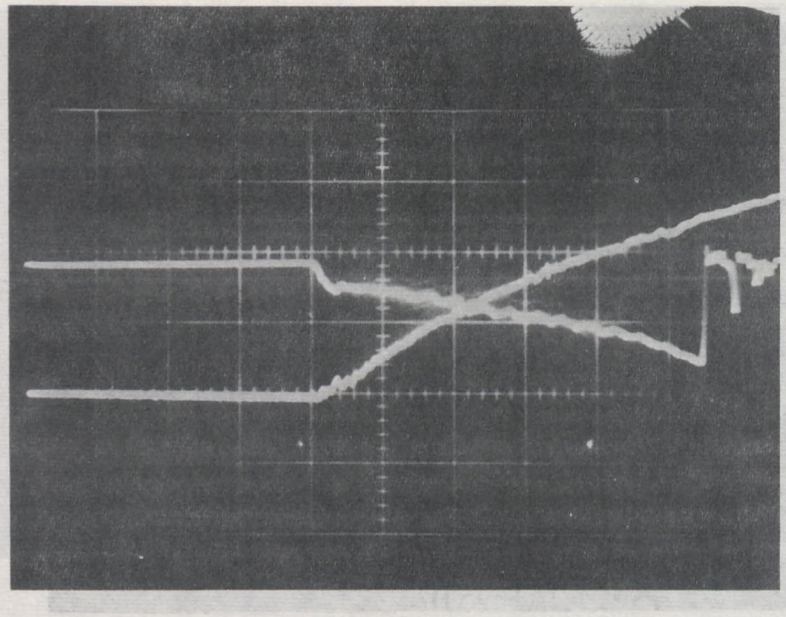

Figure 8. Oscillograph Trace of Ductile Specimen Test.

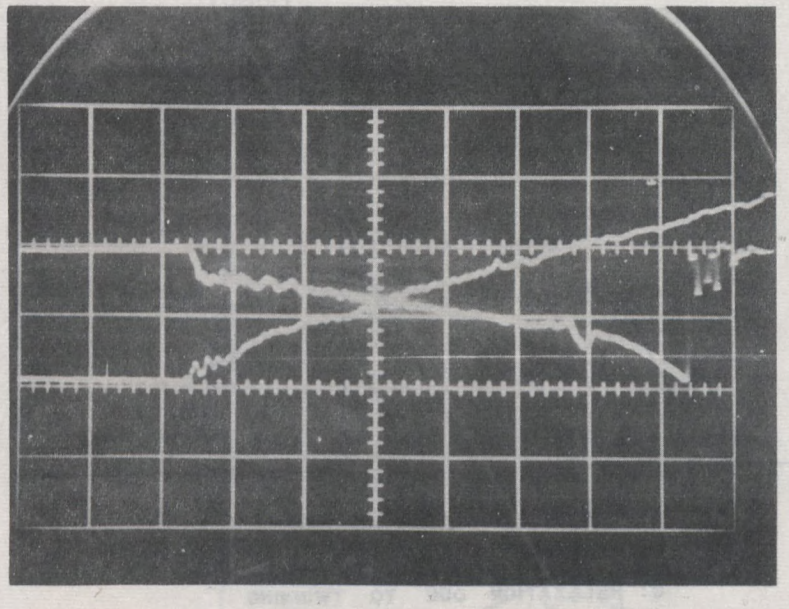

Figure 9. Oscillograph Trace of Ductile Specimen Test showing Twinning.

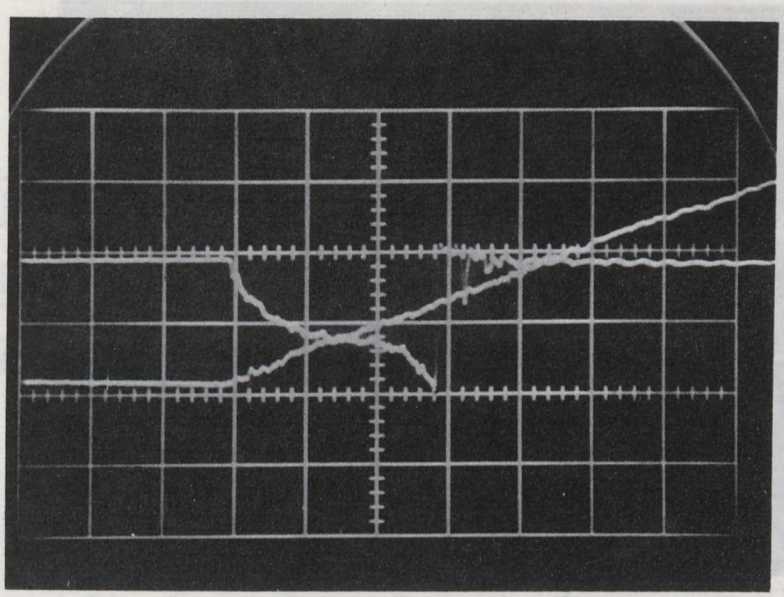

Figure 10. Oscillograph Trace of Ductile Specimen Test with Two Equal Glide Directions.

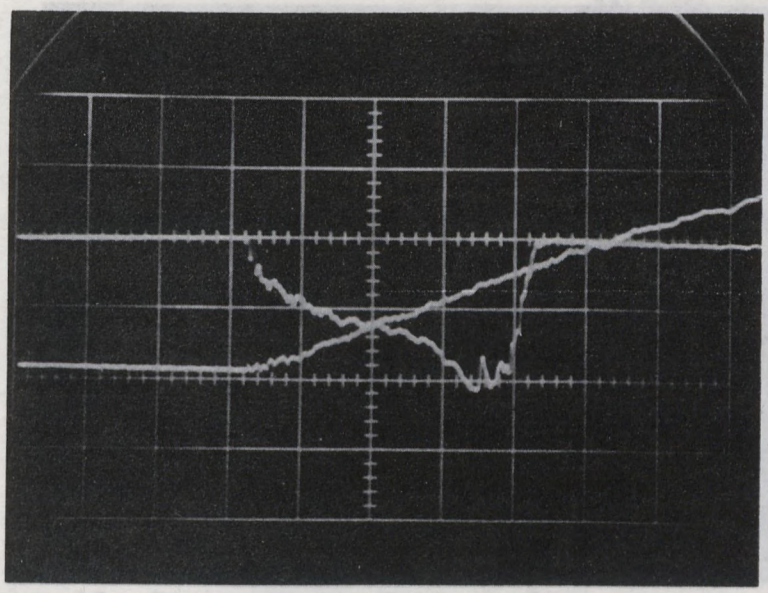

Figure 11. Oscillograph Trace of Ductile Specimen Test with Two Equal Glide Directions showing Twinning.

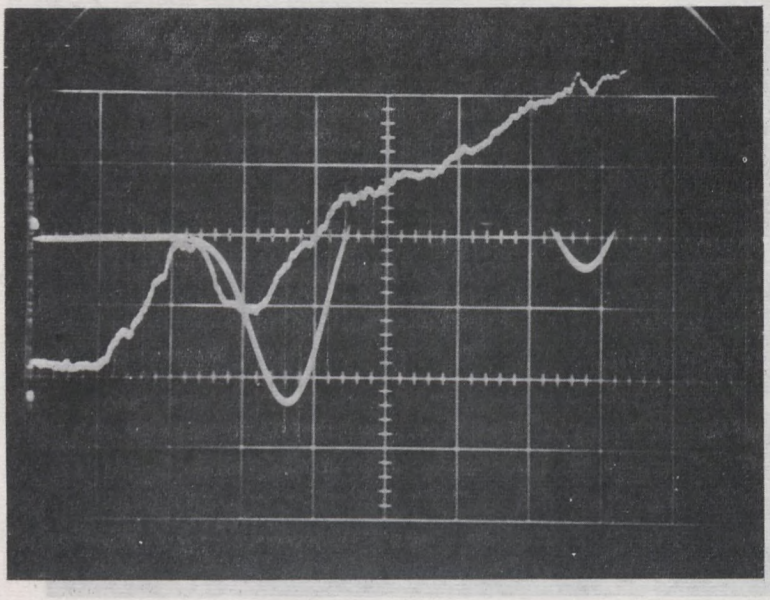

Figure 12. Oscillograph Trace showing Brittle Fracture by Pure Cleavage.

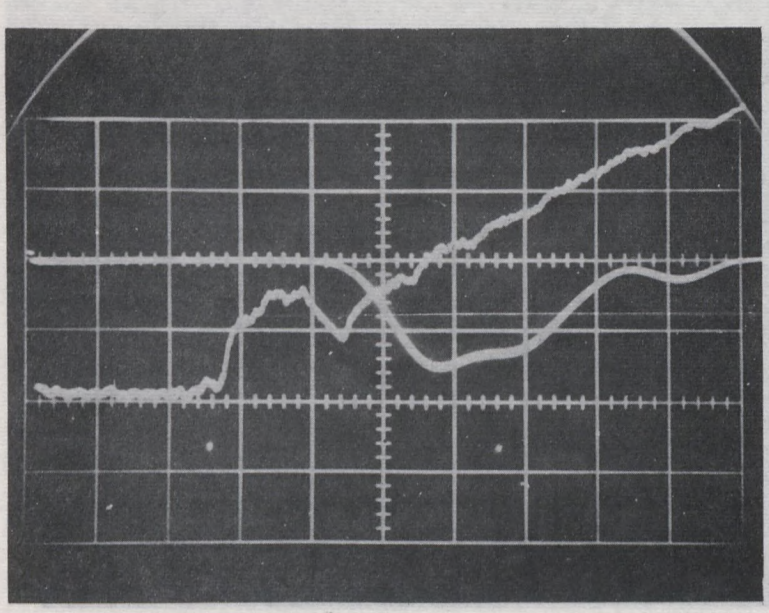

Figure 13. Oscillograph Trace showing Brittle Fracture after Small Deformation.

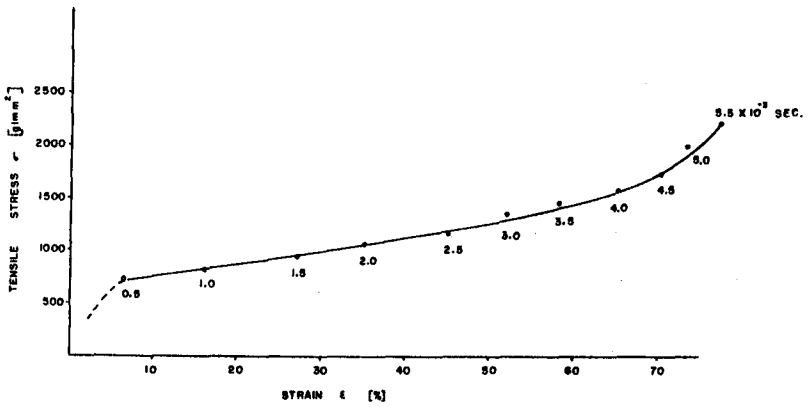

Figure 14. Stress-Strain Curve for Specimen No. 6-2.

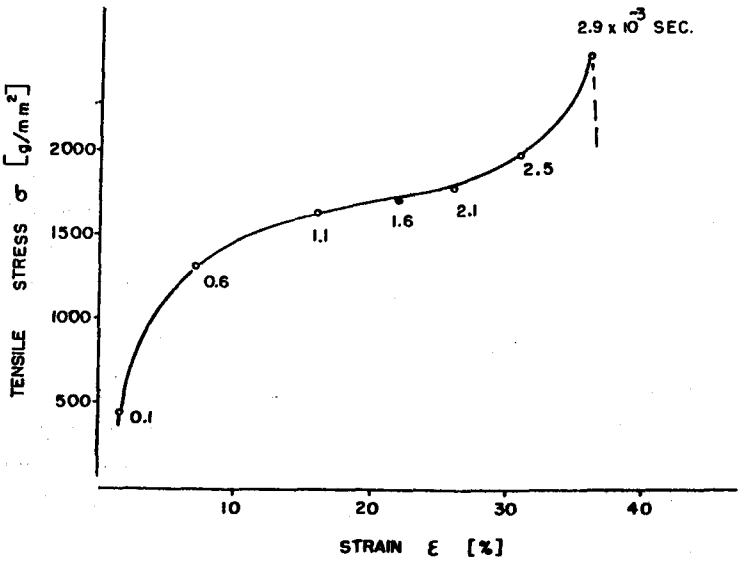

Figure 15. Stress-Strain Curve for Specimen No. 10-3.

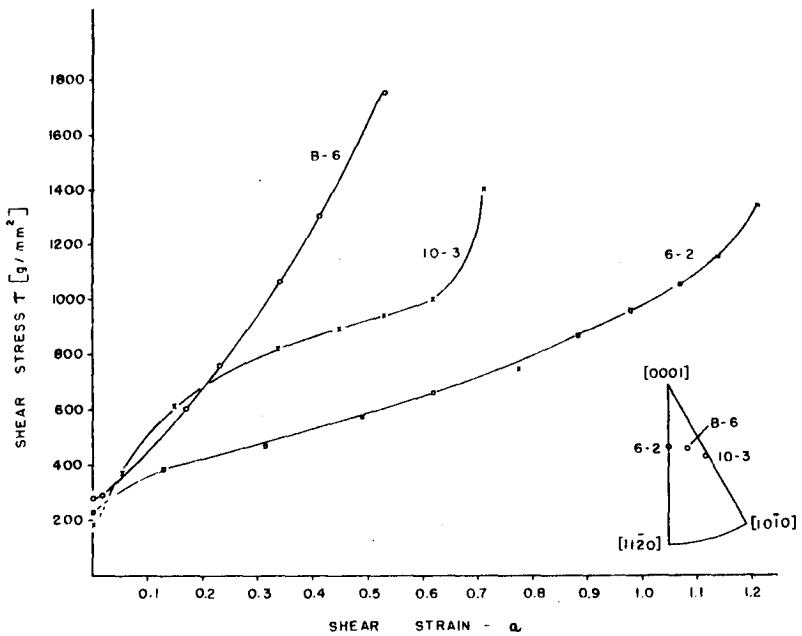

Figure 16. Resolved Shear-stress vs Shear-strain Curves.

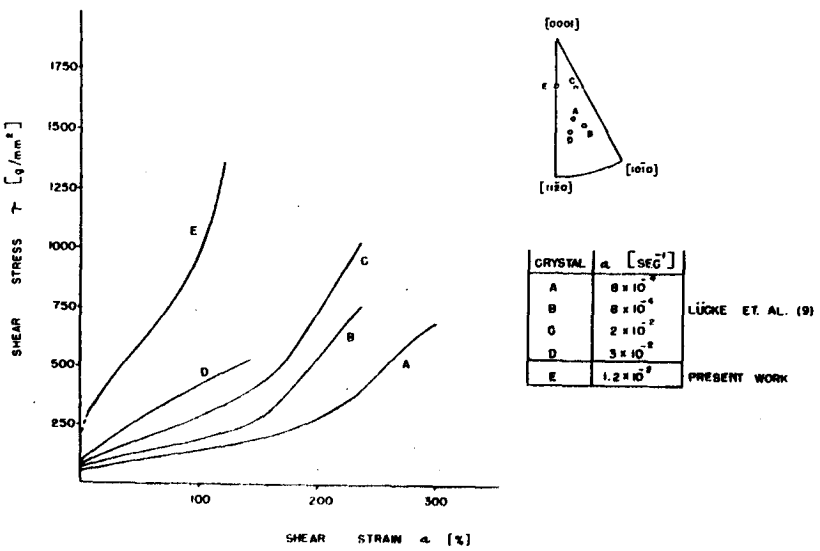

Figure 17. Comparison of Resolved Shear-stress vs Shear-strain Results.

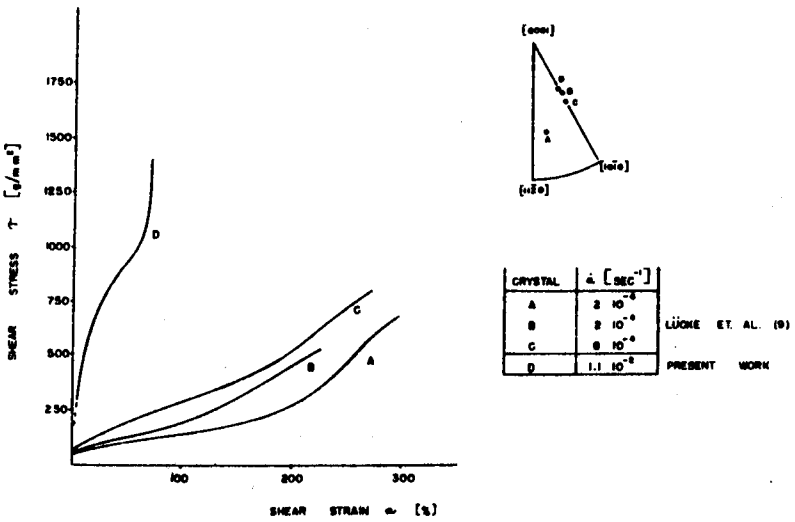

Figure 18. Comparison of Resolved Shear-stress vs Shear-strain Results.

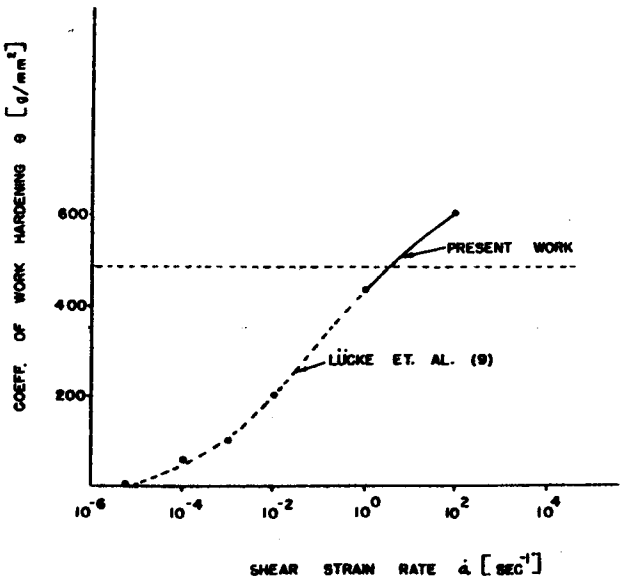

Figure 19. Coefficient of Work Hardening vs Shear-strain Rate.

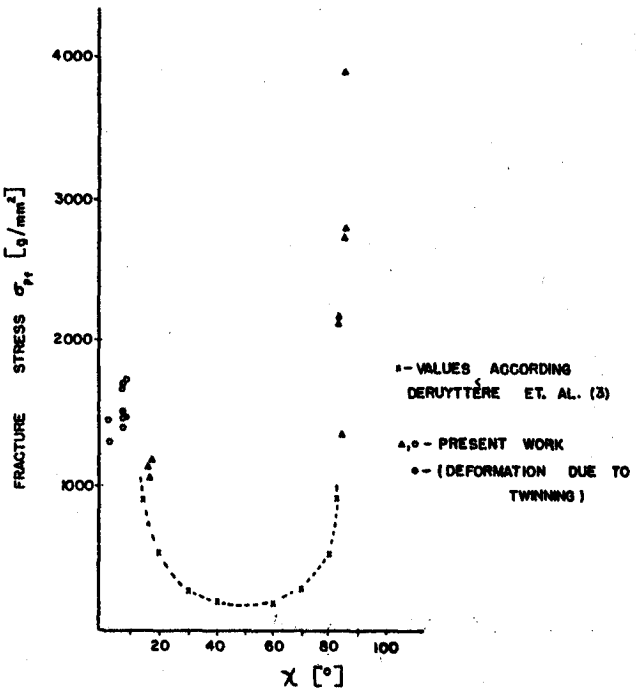

Figure 20. Fracture Stress vs Orientation.

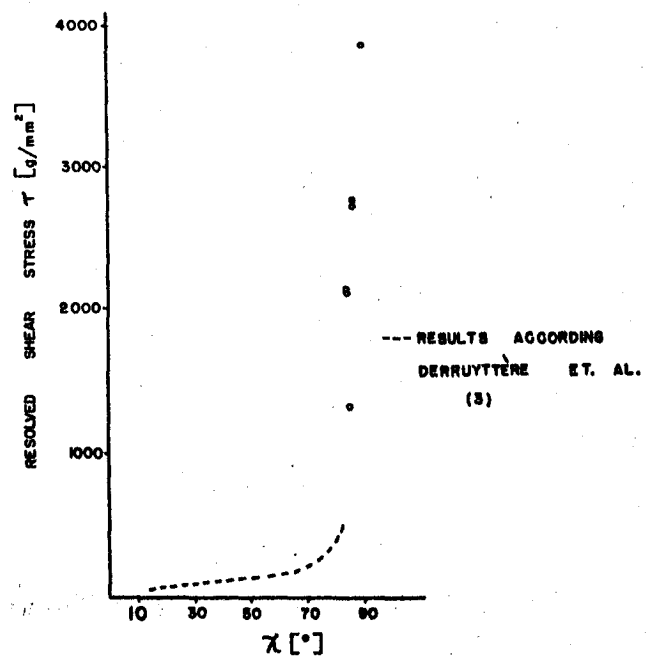

Figure 21. Resolved Shear-stress vs Orientation.

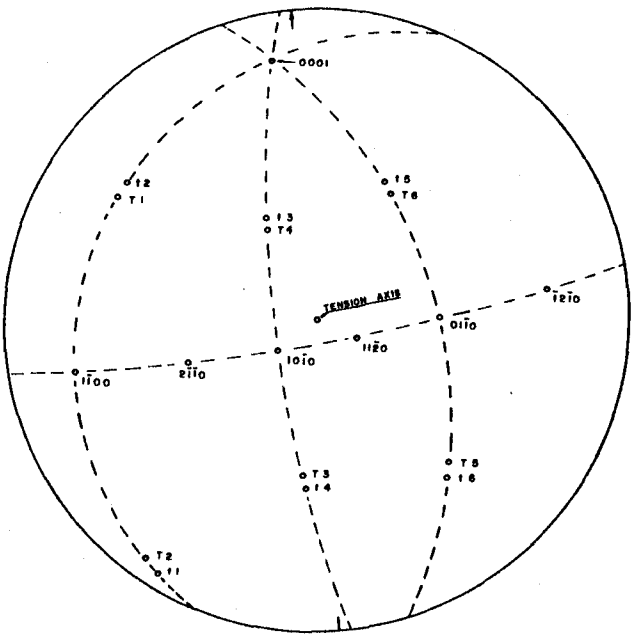

Figure 22. Stereographic Projection of Specimen No. C-3.

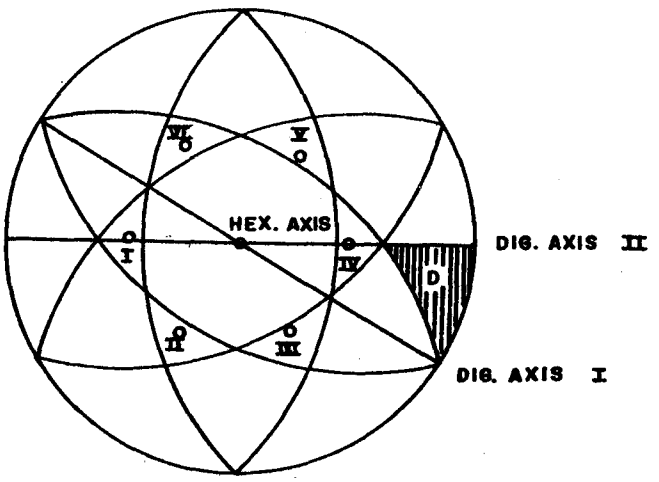

Figure 23. Schmid and Boas Numbering System for all Possible Twinning Planes.